Valley-controlled transport in graphene WSe$_2$ heterostructures under off-resonant polarized light

M. Zubair [1,*] P. Vasilopoulos,[1,†] and M. Tahir [2,‡]

[1]*Department of Physics, Concordia University, 7141 Sherbrooke Ouest, Montreal, Quebec H4B 1R6, Canada*
[2]*Department of Physics, Colorado State University, Fort Collins, Colorado 80523, USA*

We investigate the electronic dispersion and transport properties of graphene/WSe$_2$ heterostructures in the presence of a proximity-induced spin-orbit coupling λ_v, sublattice potential Δ, and an off-resonant circularly polarized light of frequency Ω that renormalizes Δ to $\bar{\Delta}_{\eta p} = \Delta + \eta p \Delta_\Omega$ with η and p the valley and polarization indices, respectively, and Δ_Ω the gap due to the off-resonant circularly polarized light. Using a low-energy Hamiltonian we find that the interplay between different perturbation terms leads to inverted spin-orbit coupled bands. At high Ω we study the band structure and dc transport using the Floquet theory and linear response formalism, respectively. We find that the inverted band structure transfers into the direct band one when the off-resonant light is present. The valley-Hall conductivity behaves as an even function of the Fermi energy in the presence and absence of this light. At $\Delta_\Omega = \lambda_v - \Delta$, a transition occurs from the valley-Hall phase to the anomalous Hall phase. In addition, the valley-Hall conductivity switches sign when the polarization of the off-resonant light changes. The valley polarization vanishes for $\Delta_\Omega = 0$ but it is finite for $\Delta_\Omega \neq 0$ and reflects the lifting of the valley degeneracy of the energy levels, for $\Delta_\Omega \neq 0$, when the off-resonant light is present. The corresponding spin polarization, present for $\Delta_\Omega = 0$, increases for $\Delta_\Omega \neq 0$. Further, pure K or K' valley polarization is generated when Δ_Ω changes sign. Also, the charge Hall conductivity is finite for $\Delta_\Omega \neq 0$ and changes sign when the handedness of the light polarization changes.

I. INTRODUCTION

Since its discovery graphene has attracted immense attention both theoretically and experimentally due to its peculiar electronic and optical properties [1]. But, it has limited usage in the field of spintronics due to its very weak intrinsic spin-orbit coupling (SOC). The intrinsic SOC in graphene is theoretically predicted to be weak, 12 μeV [2]. A value of 20 μeV is reported in a recent experiment for graphene on SiO$_2$ substrate [3]. A lot of efforts have been made to enhance the strength of SOC in graphene by employing external means, such as graphene hydrogenation [4,5] or fluorination [6], as well as heavy adatom decoration [7,8], and bringing it to proximity with other two-dimensional materials specifically transition metal dichalcogenides (TMDCs) [9–11]. In recent years the heterostructures of graphene and TMDCs have become more promising because the Dirac cone of graphene is well fit in the band gap of TMDCs, which leaves it intact. The giant native SOC of TMDCs is transferred to graphene via hybridization processes. Moreover, the combinations of graphene with TMDCs, such as MoS$_2$ or WSe$_2$, exhibit the proximity SOC on the meV scale [12–19].

Presently, SOC, induced by proximity effects, is no longer limited to theoretical studies, as it has been demonstrated by experimentally as well [20]. The breaking of spatial symmetry due to the substrate leads to an alteration of the Hamiltonian and spin degeneracy of graphene and opens a gap in its massless energy dispersion. In addition, it has been verified by experiments [19,21–23] that another type of sublattice-resolved intrinsic SOC arises, the so-called valley-Zeeman or staggered SOC with opposite sign on the *A* and *B* sublattices. Further, enhancement of the Rashba SOC and creation of staggered potentials are also unavoidable [24].

Nowadays, the optical control of functional materials has been become a hot topic in the condensed matter physics. In addition, it creates a bridge between condensed matter physics [25] and ultrafast spectroscopy [26]. Many intriguing phenomena have been realized in optically driven quantum solids such as light induced superconductivity [27,28], photo-initiated insulator-metal transition [29,30], microscopic interactions, such as the electron-phonon one, controlled by light [31–33], and theoretically predicted Floquet topological phases of matters [34–38]. These Floquet phases have stimulated much interest but direct evidence for electron-photon Floquet dressed states is scarce to date [39,40] contrary to the field of artificial lattices [41–46].

Recently, light-induced anomalous Hall effect has been observed experimentally in monolayer graphene by using an ultrafast transport technique [47] and predicted theoretically using a quantum Liouville equation with relaxation [48]. Also, graphene under the influence of light has been studied in various frameworks [34–37,49–53] The transport properties, especially valley-dependent dc transport, using the Floquet theory, has not been addressed sufficiently in contrast with a large amount of research on proximitized graphene. As far as

*muhammad.zubair@mail.concordia.ca; mzubair199@gmail.com
†p.vasilopoulos@concordia.ca
‡tahir@colostate.edu; m.tahir06@alumni.imperial.ac.uk

transport in the presence of an off-resonant light is concerned, we are aware only of an electron transport study in MoS_2 [54], of another one on graphene and the Lieb lattice [55], and of a thermal transport study in topological insulators in the absence of any SOC [56]. Here we investigate theoretically the band structure in laser-driven graphene/WSe_2 heterostructures using the Floquet theory in the high-frequency regime. Also, we study dc transport in such heterostructures in the framework of linear response theory. We show that the interplay between the proximity SOCs and off-resonant light leads to a phase transition from the inverted band regime to the direct one. Our results are in good agreement with experimental results [47] in the limit of vanishing proximity SOCs.

In Sec. II we specify the Hamiltonian and obtain the eigenvalues and eigenfunctions of the proximity modified graphene as well as an analytical expression for the density of states (DOS). In Sec. III we derive analytical expressions for the conductivities and provide numerical results. Conclusions and a summary follow in Sec. IV.

II. FORMULATION

The real space tight-binding (TB) Hamiltonian of proximitized graphene is written as [24,57,58]

$$H = -t_J \sum_{\langle i,j \rangle, \alpha} c_{i\alpha}^\dagger c_{j\alpha} + \Delta \sum_{i\alpha} \eta_{c_i} c_{i\alpha}^\dagger c_{i\alpha}$$
$$+ \frac{i}{3\sqrt{3}} \sum_{\langle\langle i,j \rangle\rangle, \alpha\alpha'} \lambda_I^i \nu_{ij} c_{i\alpha}^\dagger c_{j\alpha'} [s_z]_{\alpha\alpha'}$$
$$+ \frac{2i\lambda_R}{3} \sum_{\langle i,j \rangle, \alpha\alpha'} c_{i\alpha}^\dagger c_{j\alpha'} [(s \times \hat{\mathbf{d}}_{ij})_z]_{\alpha\alpha'}. \quad (1)$$

Here t_J is the hopping parameter, $c_{i\alpha}^\dagger$ creates an electron with spin polarization α at site i that belongs to sublattice A or B, and $\langle i,j \rangle$ ($\langle\langle i,j \rangle\rangle$) runs over the nearest (second nearest) neighboring sites. The second term is a staggered on-site potential, which takes into account the effective energy difference experienced by atoms at the lattice sites A ($\eta_{c_i} = +1$) and B ($\eta_{c_i} = -1$), respectively. The third and fourth terms represent the proximity-induced enhancement of the spin-orbit coupling (SOC) due to a weak hybridization with the heavy atoms in TMDCs. The third term is the sublattice resolved intrinsic SOC (λ_I^i with $i = A, B$) where $\nu_{ij} = +1$, if the second nearest hopping is anticlockwise, and $\nu_{ij} = -1$ if it is clockwise with respect to the positive z axis. The last term is the Rashba SOC parametrized by λ_R. It arises because the inversion symmetry is broken when the graphene sheet is placed on top of TMDCs. Further, $s = (s_x, s_y, s_z)$ is the Pauli spin matrix and $\hat{\mathbf{d}}_{ij}$ is the unit vector connecting the sites i and j in the same sublattice.

We analyze the physics of electrons near the Fermi energy using a low-energy effective Hamiltonian derived from Eq. (1) and a Dirac theory around K and K' points. It reads [59–61]

$$H_{s_z\eta} = v_F(\eta\sigma_x p_x + \sigma_y p_y) + \Delta\sigma_z + \lambda_R(\eta s_y\sigma_x - s_x\sigma_y)$$
$$+ \frac{1}{2}[\lambda_I^A(\sigma_z + \sigma_0) + \lambda_I^B(\sigma_z - \sigma_0)]\eta s_z. \quad (2)$$
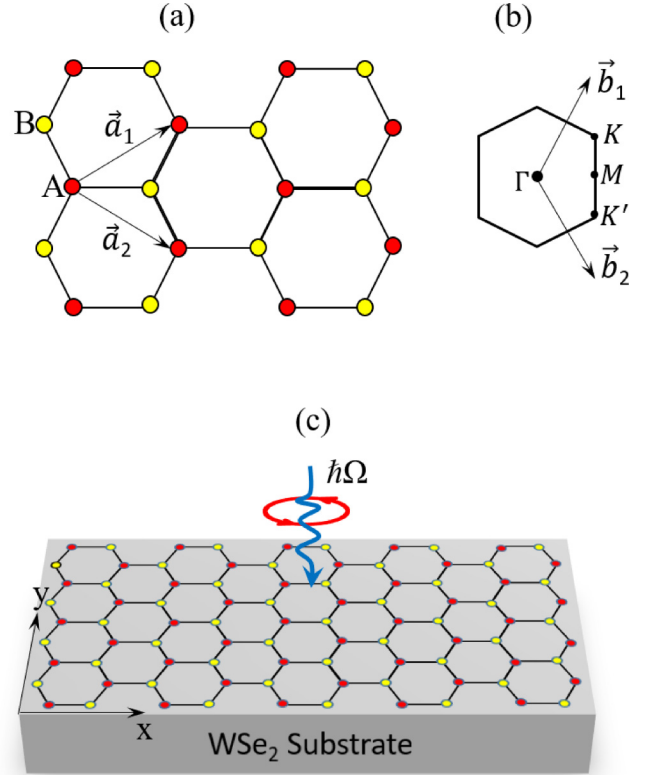

FIG. 1. (a) Real-space graphene with $\vec{a}_1$ and $\vec{a}_2$ the primitive lattice vectors. (b) Graphene's first Brillouin zone and high symmetry points Γ, K, K', and M in reciprocal space. Its primitive lattice vectors are $\vec{b}_1$ and $\vec{b}_2$. (c) Schematics of graphene epitaxially grown on a WSe_2 substrate and irradiated by a left circularly polarized light.

Here $\eta = +1(-1)$ denotes the valley K (K'), Δ is the mass term that breaks the inversion symmetry, λ_R the Rashba type SOC strength, $\sigma = (\sigma_x, \sigma_y, \sigma_z)$ the Pauli matrix that corresponds to the pseudospin (i.e., $A - B$ sublattice), σ_0 is the unit matrix in the sublattice space, and v_F (8.2×10^5 m/s) denotes the Fermi velocity of Dirac fermions. The last term arises due to the breaking of sublattice symmetry and can be categorized into two groups according to its dependence on sublattice spin: (i) $\lambda_{so}\sigma_z\eta s_z$ when $\lambda_{so} = (\lambda_I^A + \lambda_I^B)/2$. This is called conventional Kane-Mele (KM) type SOC, which has a magnitude of the order of μeV in graphene/TMDCs heterostructures [2,24,61]. (ii) $\lambda_v\sigma_0\eta s_z$ when $\lambda_v = (\lambda_I^A - \lambda_I^B)/2$. It is called valley-Zeeman or staggered SOC and has been experimentally confirmed in graphene on TMDCs [19,21–23]; it occurs only for $\lambda_I^A = -\lambda_I^B$. Further, Refs. [2,24,61] show that λ_{so} is negligibly small or zero. In view of that, we treat only the regime $\lambda_v \gg \lambda_{so}$ and neglect λ_{so} altogether. As shown in Fig. 1, monolayer graphene, irradiated by off-resonant circularly polarized light, is grown on WSe_2 that provides a staggered potential and induces SOC in graphene. We study the changes induced by circularly polarized light in graphene/WSe_2 in the presence of a perpendicular electric field E. We describe the monochromatic light through a time-dependent vector potential $\vec{A}(t) = (E_0/\Omega)(\cos\Omega t, p\sin\Omega t)$ with Ω its frequency, E_0 the amplitude of the field E, and $p = +1(-1)$ for left (right) circular polarization. The vector

potential is periodic in time $A(t + T) = A(t)$ with $T = 2\pi/\Omega$. For high frequencies $\hbar\Omega \gg t_J$ and low light intensities, i.e., $\mathcal{A}^2 << 1$ with $\mathcal{A} = ev_F E_0/\hbar\Omega$ characterizing the intensity of light, Eq. (2) gives the Hamiltonian

$$H_{s\eta}(t) = H_{s\eta}^0 + V(t), \quad (3)$$

with

$$H_{s_z\eta}^0 = v_F(\eta\sigma_x p_x + \sigma_y p_y) + \Delta\sigma_z + \lambda_v\sigma_0\eta s_z$$
$$+\lambda_R(\eta s_y\sigma_x - s_x\sigma_y),$$
$$V(t) = -(ev_F/\hbar)[\eta\sigma_x A_x(t) + \sigma_y A_y(t)]. \quad (4)$$

For $\hbar\Omega \gg t_J$ and $\mathcal{A}^2 << 1$, Eq. (3) can be reduced to an effective, time-independent Hamiltonian $H_{s_z\eta}^{\text{eff}}(t)$ using Floquet theory [35]. $H_{s\eta}^{\text{eff}}(t)$ is defined through the time evolution operator over one period

$$\hat{U} = \hat{T}\exp[-i\int_0^T H_{s_z\eta}(t)dt] = \exp\big[-iH_{s_z\eta}^{\text{eff}}T\big], \quad (5)$$

where $\hat{T}$ is time ordering operator. Using perturbation theory and expanding $\hat{U}$ in the limit of large frequency Ω, we obtain

$$H_{s_z\eta}^{\text{eff}} = H_{s_z\eta}^0 + [V_{-1}, V_1]/\hbar\Omega + O(\Omega^{-2}), \quad (6)$$

where $V_m = (1/T)\int_0^T e^{-im\Omega t}V(t)dt$ is the mth Fourier harmonic of the time-periodic Hamiltonian and $[V_{-1}, V_1]$ the commutator between V_{-1} and V_1. Corrections to Eq. (6), to all orders of $1/\Omega$, can be obtained by the method of Ref. [55]. Here we neglect them because we treat only the case $\hbar\Omega \gg t_J$. Using Eqs. (3) and (6) we obtain

$$H_{s_z\eta}^{\text{eff}} = v_F[\eta\sigma_x p_x + \sigma_y p_y] + \bar{\Delta}_{\eta p}\sigma_z + \lambda_v\sigma_0\eta s_z$$
$$+\lambda_R(\eta s_y\sigma_x - s_x\sigma_y), \quad (7)$$

where $\bar{\Delta}_{\eta p} = \Delta + \eta p\Delta_\Omega$ with $\Delta_\Omega = v_F^2 e^2 E_0^2/\hbar\Omega^3$; $\bar{\Delta}_{\eta p}$ is the renormalized mass term due to the circularly polarized light, which creates a gap Δ_Ω in pure graphene, i.e., for $\Delta = 0$, see Ref. [35].

The diagonalization of Eq. (7) gives the dispersion

$$E_\xi^{\eta p}(k) = l\big\{G_\eta + 2\lambda_R^2 + \epsilon_k^2 + 2s\sqrt{\Upsilon}\big\}^{1/2}, \quad (8)$$

where $\xi = \{l, s\}$ and $G_\eta = \lambda_v^2 + \bar{\Delta}_{\eta p}^2$, $\Upsilon = \epsilon_k^2\bar{\lambda}^2 + (\lambda_R^2 - \lambda_v\bar{\Delta}_{\eta p})^2$ with $\epsilon_k = \hbar v_F k$, $\bar{\Delta}_{\eta p} = \Delta + \eta p\Delta_\Omega$ and $\bar{\lambda}^2 = \lambda_R^2 + \lambda_v^2$. Further, $l = +1(-1)$ denotes the conduction (valence) band and $s = +1(-1)$ represents the spin-up (spin-down) branches and is not a Pauli matrix s_z. The normalized eigenfunctions for both valleys are

$$\psi_\xi^{+p}(k) = \frac{N_\xi^{+p}}{\sqrt{S_0}}\begin{pmatrix} 1 \\ A_\xi^{\eta p}e^{i\phi} \\ -iB_\xi^{\eta p}e^{i\phi} \\ -iC_\xi^{\eta p}e^{2i\phi} \end{pmatrix}e^{i\mathbf{k}\cdot\mathbf{r}}, \quad (9)$$

$$\psi_\xi^{-p}(k) = \frac{N_\xi^{-p}}{\sqrt{S_0}}\begin{pmatrix} -A_\xi^{\eta p}e^{i\phi} \\ 1 \\ iC_\xi^{\eta p}e^{2i\phi} \\ -iB_\xi^{\eta p}e^{i\phi} \end{pmatrix}e^{i\mathbf{k}\cdot\mathbf{r}}, \quad (10)$$

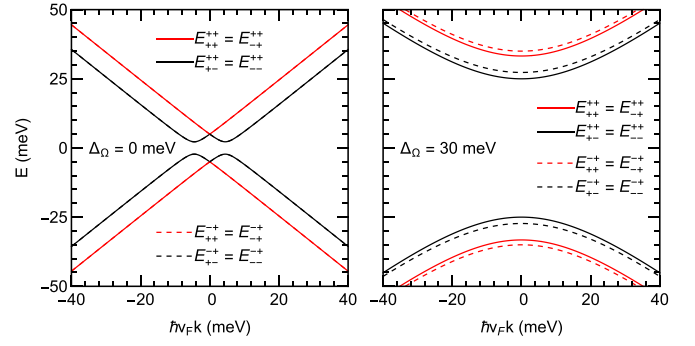FIG. 2. Energy dispersion curves around K and K' of a graphene/WSe$_2$ heterostructure for $\Delta = 1$ meV, $\lambda_v = 4$ meV, and $\lambda_R = 2$ meV. The left panel shows the inverted band regime, with strong spin mixing of different states, obtained for $\Delta_\Omega < \Delta + \lambda_v$. The right panel shows the direct band regime, with nearly full spin polarization, obtained for $\Delta_\Omega > \Delta + \lambda_v$. The marking of all curves resulting from Eq. (8), with $p = 1$ for all of them, is shown inside the panels. The solid-black (red) curves are for $\eta = +1$ and $s = +1(-1)$ and the dashed-black (red) ones for $\eta = -1$ and $s = +1(-1)$, respectively, with

$$N_\xi^{\eta p} = l\big[1 + (A_\xi^{\eta p})^2 + (B_\xi^{\eta p})^2 + (C_\xi^{\eta p})^2\big]^{-1/2}, \quad (11)$$

$S_0 = L_x L_y$ the area of the sample, and $\phi = \tan^{-1}(k_y/k_x)$. Further, $A_\xi^{\eta p} = \{E_\xi^{\eta p} - \eta\alpha_1^\eta\}/\epsilon_k$, $B_\xi^{\eta p} = 2\lambda_R\{(E_\xi^{\eta p})^2 - (\alpha_1^\eta)^2\}/\epsilon_k\{(E_\xi^{\eta p} + \eta\alpha_1^\eta)(E_\xi^{\eta p} - \eta\alpha_2^\eta) - \epsilon_k^2\}$, and $C_\xi^{\eta p} = 2\lambda_R\{E_\xi^{\eta p} - \eta\alpha_1^\eta\}/\{(E_\xi^{\eta p} + \eta\alpha_1^\eta)(E_\xi^{\eta p} - \eta\alpha_2^\eta) - \epsilon_k^2\}$ with $\alpha_1^\eta = \bar{\Delta}_{\eta p} + \lambda_v$, and $\alpha_2^\eta = \bar{\Delta}_{\eta p} - \lambda_v$.

In numerical calculations throughout the paper, we use values of the parameters Δ, λ_v, and λ_R somewhat larger than those of [57] to have well-resolved spin and valley splittings since the overall physics of the system is not changed when we do so. As for the values of Δ_Ω, it is known that the off-resonant light does not directly excite the electrons; instead, it modifies the electron bands through virtual photon absorption processes. To study the topological transitions of bands, this light must satisfy the condition $\hbar\Omega \gg t_J$ and $\mathcal{A}^2 << 1$. Accordingly, we will use the values of Δ_Ω from Refs. [35,47,54].

The typical band structure (8) for both valleys is illustrated in Fig. 2 for $p = +1$, $\Omega_\Omega < \Delta + \lambda_v$ (inverted band regime), and $\Delta_\Omega > \Delta + \lambda_v$ (direct band regime). The left panel shows the inverted band regime. The inversion occurs due to the anticrossing of the bands with opposite spins and in the presence of the Rashba SOC. The right panel depicts the direct band regime with simple parabolic dispersion. It is found that the spin and valley degeneracies are completely lifted when $\Delta_\Omega > \Delta + \lambda_v$, whereas the valley degeneracy is restored in the opposite limit similar to silicene [62]. The valleys are interchanged if proximitized graphene is irradiated by a right circularly polarized light $p = -1$ (not shown here).

A. Limiting cases and density of states (DOS)

(i) Setting $\Delta = 0$ in Eq. (8), we obtain

$$E_\xi^{\eta p}(k) = l\big\{\lambda_v^2 + \Delta_\Omega^2 + 2\lambda_R^2 + \epsilon_k^2 + 2s\sqrt{Y}\big\}^{1/2}, \quad (12)$$

with $Y = \epsilon_k^2\bar{\lambda}^2 + (\lambda_R^2 - \eta\lambda_v\Delta_\Omega)^2$.
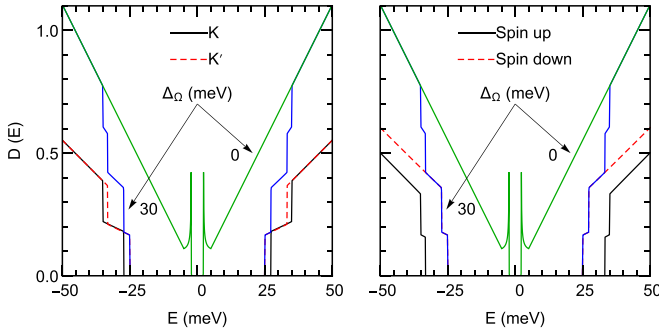
FIG. 3. Density of states for two values of Δ_Ω, as indicated, and $\Gamma = 0.01$ meV. The left panel shows the valley components of the DOS, with both spins included, whereas the right panel shows the spin components of the DOS, with both valleys included. In both panels the curves indicated by arrows show the total DOS. The parameters Δ, λ_v, and λ_R are the same as in Fig. 2. The marking of the curves is shown inside the panels. In the left panel both spin contributions are included, in the right one both valley contributions are included.

(ii) In the limit $\lambda_R = 0$, Eq. (8) reduces

$$E_\xi^{\eta p}(k) = l\big[\epsilon_k^2 + \bar{\Delta}_{\eta p}^2\big]^{1/2} + s\lambda_v. \qquad (13)$$

The DOS per unit area corresponding to Eq. (8) is given by

$$D(E) = \frac{|E|v_F^{-2}}{2\pi\hbar^2} \sum_{\eta p} \left[\frac{\theta(|E| - |E_{1g}^{\eta p}|)}{1 - \bar{\lambda}/M^+} + \frac{\theta(|E| - |E_{2g}^{\eta p}|)}{1 + \bar{\lambda}/M^-} \right], \quad (14)$$

with

$$E_{1g}^{\eta p} = \lambda_v + \bar{\Delta}_{\eta p}, \quad E_{2g}^{\eta p} = \big[(\lambda_v - \bar{\Delta}_{\eta p})^2 + 4\lambda_R^2\big]^{1/2},$$

$$M^\pm = \big[(\lambda_R^2 - \lambda_v\bar{\Delta}_{\eta p})^2 + \hbar^2 v_F^2 \bar{\lambda}^2 \epsilon_\pm\big]^{1/2}, \qquad (15)$$

$$\hbar^2 v_F^2 \epsilon_\pm = E^2 + \lambda_v^2 - \bar{\Delta}_{\eta p}^2 \pm 2\big[\bar{\lambda}^2 E^2 - \lambda_R^2(\lambda_v + \bar{\Delta}_{\eta p})^2\big]^{1/2}.$$

In Fig. 3 we plot the DOS given by Eq. (14). The two jumps in the DOS indicate that two gaps open at each valley, displaying the clear signature of lifting the spin and valley degeneracies, when graphene on WSe$_2$ substrate is in the direct band regime. The spin and valley degeneracies are completely lifted in the direct band regime while only the spin degeneracy is lifted in the inverted band regime. Note that the DOS diverges in the inverted band regime as $D(E) \propto (E - \Delta_1)^{-1/2}$ with $\Delta_1 = \lambda_R(\lambda_v + \Delta)/(\lambda_R^2 + \lambda_v^2)^{1/2}$ (see green curves in both panels). This divergence is due to the Mexican-hat energy dispersion [63], cf. Fig. 2. In passing we may add that this behavior of the DOS remains the same as the broadened one provided the level width Γ is small, $\Gamma < 0.5$ meV. For higher Γ the small structure of the DOS curves is smoothened out.

III. CONDUCTIVITIES

We consider a many-body system described by the Hamiltonian $H = H_0 + H_I - \mathbf{R} \cdot \mathbf{F(t)}$, where H_0 is the unperturbed part, $H_I = \lambda V$ is a binary-type interaction (e.g., between electrons and impurities or phonons) of strength λ, and $-\mathbf{R} \cdot \mathbf{F}(t)$ is the interaction of the system with the external field $F(t)$ [64]. For conductivity problems we have $\mathbf{F}(t) = e\mathbf{E}(t)$, where

$\mathbf{E}(t)$ is the electric field, e the electron charge, $\mathbf{R} = \sum_i \mathbf{r}_i$, and $\mathbf{r}_i$ the position operator of electron i. In the representation in which H_0 is diagonal the many-body density operator $\rho = \rho^d + \rho^{nd}$ has a diagonal part ρ^d and a nondiagonal part ρ^{nd}. Using $\rho = e^{-\beta H}$ and $H = H_0 + \lambda V$, all operators were evaluated in the van Hove limit, $\lambda \to 0$, $t \to \infty$ but $\lambda^2 t$ finite, and all averages $<X> = Tr\{X\rho\}$ in the representation in which H_0 is diagonal. In this representation λV is assumed nondiagonal; if it has a diagonal part, it's included in H_0. Correspondingly, for weak electric fields and weak scattering potentials, for which the first Born approximation applies, the conductivity tensor has a diagonal part $\sigma_{\mu\nu}^d$ and a nondiagonal part $\sigma_{\mu\nu}^{nd}$; the total conductivity is $\sigma_{\mu\nu}^{tot} = \sigma_{\mu\nu}^d + \sigma_{\mu\nu}^{nd}$, $\mu, \nu = x, y$. For further details see Ref. [64].

In general we have two kinds of currents, diffusive and hopping, with $\sigma_{\mu\nu}^d = \sigma_{\mu\nu}^{dif} + \sigma_{\mu\nu}^{col}$, but usually only one of them is present. The term $\sigma_{\mu\nu}^{col}$ was introduced in Ref. [64] to distinguish collisional current contributions that are different from the standard diffusive ones valid for elastic scattering and characterized by a relaxation time τ. As such, this is the main term for transport in a magnetic field when the diffusion contributions vanish. It also describes hopping between localized states. If no magnetic field is present, the hopping term $\sigma_{\mu\nu}^{col}$ vanishes identically and only the term $\sigma_{\mu\nu}^{dif}$ survives. For elastic scattering it is given by [64]

$$\sigma_{\mu\nu}^d = \frac{\beta e^2}{S_0} \sum_\zeta f_\zeta(1 - f_\zeta)v_{\nu\zeta}\, v_{\mu\zeta}\, \tau_\zeta, \qquad (16)$$

with τ_ζ the momentum relaxation time, and $v_{\mu\zeta}$ the diagonal matrix elements of the velocity operator. Further, $f_\zeta = [1 + \exp[\beta(E_\zeta - E_F)]]^{-1}$ is the Fermi-Dirac distribution function, $\beta = 1/k_B T$, and T the temperature.

Regarding the contribution $\sigma_{\mu\nu}^{nd}$ one can use the identity $f_\zeta(1 - f_{\zeta'})[1 - \exp[\beta(E_\zeta - E_{\zeta'})]] = f_\zeta - f_{\zeta'}$ and cast the original form [64] in the more familiar one

$$\sigma_{\mu\nu}^{nd} = \frac{i\hbar e^2}{S_0} \sum_{\zeta \neq \zeta'} \frac{(f_\zeta - f_{\zeta'})\, v_{\nu\zeta\zeta'}\, v_{\mu\zeta\zeta'}}{(E_\zeta - E_{\zeta'})(E_\zeta - E_{\zeta'} - i\Gamma)}, \qquad (17)$$

where the sum runs over all quantum numbers ζ and ζ' with $\zeta \neq \zeta'$. The infinitesimal quantity ϵ, in the original form of the conductivity, has been replaced by Γ_ζ to phenomenologically account for the broadening of the energy levels. One should keep in mind that a *strong* disorder may modify the Hall conductivity considerably. However, this problem is not studied here. In Eq. (17) $v_{\nu\zeta\zeta'}$ and $v_{\mu\zeta\zeta'}$ are the off-diagonal matrix elements of the velocity operator. The relevant velocity operators are given by $v_x = \partial H/\hbar\partial k_x$ and $v_y = \partial H/\hbar\partial k_y$. With $\zeta = \{l, s, k, \eta, p\} = \{\xi, k, \eta, p\}$ for brevity, they read

$$\langle\zeta|v_x|\zeta'\rangle = v_F N_\xi^{\eta p} N_{\xi'}^{\eta p}\big(D_{\xi,\xi'}^{\eta p}e^{i\phi} + F_{\xi,\xi'}^{\eta p}e^{-i\phi}\big)\delta_{\eta,\eta'}\delta_{k,k'}, \quad (18)$$

$$\langle\zeta'|v_y|\zeta\rangle = iv_F N_\xi^{\eta p} N_{\xi'}^{\eta p}\big(D_{\xi,\xi'}^{\eta p}e^{-i\phi} - F_{\xi,\xi'}^{\eta p}e^{i\phi}\big)\delta_{\eta,\eta'}\delta_{k,k'}, \quad (19)$$

where $D_{\xi,\xi'}^{\eta p} = A_{\xi'}^{\eta p} + B_\xi^{\eta p}C_{\xi'}^{\eta p}$ and $F_{\xi,\xi'}^{\eta p} = A_\xi^{\eta p} + B_{\xi'}^{\eta p}C_\xi^{\eta p}$.

The diagonal velocity matrix elements $v_{x\zeta} = \partial E^{\eta p}_{\xi}/\hbar \partial k_x$ from Eq. (8) can be readily found

$$v_{x\zeta} = \frac{l\hbar v_F^2 k_x}{E^{\eta p}_{\xi}}\left[1 + \frac{s\bar{\lambda}^2}{\sqrt{\Upsilon}}\right]. \qquad (20)$$

The above mentioned general expressions for conductivities are modified for Floquet theory [34] but are still valid for driven systems in the limit of large frequencies and weak intensity of light ($\mathcal{A} << 1$) since only the zeroth level of the Floquet states contributes [35], cf. Sec. III. Thus, these states can be taken as the eigenstates of Eq. (6). In addition, although Eq. (6) is perturbative in Ω, the above Hall conductivities expressions are nonperturbative in Ω; that is, an infinitesimal gap $\bar{\Delta}_{\eta p}$ is sufficient to yield a topological band with a quantized Hall conductance in units of $2e^2/h$ [35]. Further, the Fermi distribution is nonuniversal for systems, which are out of equilibrium but for some cases of system-bath couplings [65], the steady-state distribution becomes thermal, and we restrict our results to such cases. Additionally, the electrode chemical potential will be small, for linear responses, compared to the intrinsic chemical potential of the system, and so we ignore the electrode chemical potential in our calculations. This allows us to write the chemical potential in the Kubo formalism as a constant, i.e., without accounting for sources at the boundaries. Also, it is worth pointing out that our approach for evaluating the conductivity tensor is the same or similar with that followed in Refs. [54] for MoS$_2$, [66,67] for silicene, and [68] for WSe$_2$. In all of them a perpendicular electric field, not the source-to-drain one, was included in H_0. This is similar to our inclusion of the off-resonant light term $V(t)$ in H_0, as in the present paper, and was also the case of Ref. [56].

We now calculate the conductivity σ^{nd}_{yx} given by Eq. (17). Further, the velocity matrix elements (18) and (19) are diagonal in k, therefore k will be suppressed in order to simplify the notation. The summation in Eq. (17) runs over all quantum numbers ξ, ξ', η, η', and k. The parameter $\Gamma_{\zeta} = \Gamma^{\xi\xi'}_{\eta\eta'}$, that takes into account the level broadening, is assumed independent of the band and valley indices, i.e., $\Gamma^{\xi\xi'}_{\eta\eta'} = \Gamma$. Using Eqs. (18) and (19) we can express Eq. (17) as

$$\mathrm{Re}\sigma^{nd}_{yx}(\xi, \xi', \eta, p) = \frac{2e^2\hbar^2 v_F^2}{h}\int dk k \frac{(N^{\eta p}_{\xi}N^{\eta p}_{\xi'})^2(f^{\eta p}_{\xi k} - f^{\eta p}_{\xi'k})}{(\Delta^{\eta p}_{\xi\xi'})^2 + \Gamma^2}$$
$$\times\left[(D^{\eta p}_{\xi,\xi'})^2 - (F^{\eta p}_{\xi,\xi'})^2\right],$$
$$\mathrm{Im}\sigma^{nd}_{yx}(\xi, \xi', \eta, p) = 0, \qquad (21)$$

where $\Delta^{\eta p}_{\xi\xi'} = E^{\eta p}_{\xi k} - E^{\eta p}_{\xi'k}$.

For $\lambda = \Delta = \Delta_{\Omega} = 0$ and $\lambda_R \neq 0$, Eq. (21) vanishes because the factor $(D^{\eta p}_{\xi,\xi'})^2 - (F^{\eta p}_{\xi,\xi'})^2$ becomes zero. Ignoring skew and intervalley scatterings, the valley-Hall conductivity (σ^v_{yx}) obtained from Eq. (21) can be evaluated as

$$\sigma^v_{yx} = \sum_{\xi\xi'p}\left[\sigma^{nd}_{yx}(\xi, \xi', +, p) - \sigma^{nd}_{yx}(\xi, \xi', -, p)\right], \qquad (22)$$

where we set $\mathrm{Re}\sigma^{nd}_{yx}(\xi, \xi', \eta, p) \equiv \sigma^{nd}_{yx}(\xi, \xi', \eta, p)$. The spin-Hall conductivity σ^s_{yx} corresponding to Eq. (21) is finite only when both KM and staggered SOCs are present [69]. Therefore, σ^s_{yx} vanishes even in the presence of Rashba SOC. Even

if it does not in graphene on WSe$_2$, it is assumed negligible in the regime $\lambda_v \gg \lambda_{so}$ that we treat and we neglect it altogether, see also Sec. II, above Eq. (3). As usual, we have to multiply σ^v_{yx} by $1/2e$ [58].

We can find a simple analytical result from Eq. (22) for the specific case $\lambda_v, \lambda_R = 0$ in the low temperature limit. It is

$$\sigma^v_{yx} = \begin{cases} \dfrac{e}{2h}, & -(\Delta + \eta p\Delta_{\Omega}) < E_F < \Delta + \eta p\Delta_{\Omega} \\[2mm] \dfrac{e}{2h}\dfrac{\eta\Delta + p\Delta_{\Omega}}{E_F}, & E_F > \Delta + \eta p\Delta_{\Omega}. \end{cases} \qquad (23)$$

Equations (16) and (17) of Ref. [54] in the limit $\lambda \to 0$ are similar to Eq. (23). For $\Delta_{\Omega} \to 0$, Eq. (23) reduces to a result reported in Ref. [70]. Further, we find the charge Hall conductivity

$$\sigma^c_{yx} = \sum_{p\eta\eta'\xi\xi'}\sigma^{nd}_{yx}(\xi, \xi', \eta, \eta', p) = \begin{cases} 0, & \Delta_{\Omega} = 0 \\ \neq 0, & \Delta_{\Omega} \neq 0. \end{cases} \qquad (24)$$

In the limit $\Delta_{\Omega} \to 0$, σ^c_{yx} vanishes.

We now consider the diagonal component σ^d_{xx} given by Eq. (16). Using Eq. (18), with $\xi = \xi'$, we obtain

$$\sigma^d_{xx}(\xi, \eta, p) = \frac{e^2 v_F^2 \beta}{\pi}\int dkk\left(N^{\eta p}_{\xi}\right)^4 f^{\eta p}_{\xi k}\left(1 - f^{\eta p}_{\xi k}\right)$$
$$\times\left(A^{\eta p}_{\xi} + B^{\eta p}_{\xi}C^{\eta p}_{\xi}\right)^2 \tau^{\eta p}_{\xi k}. \qquad (25)$$

At very low temperatures we can make the approximation $\beta f^{\eta p}_{\xi k}(1 - f^{\eta p}_{\xi k}) \approx \delta(E^{\eta p}_{\xi} - E_F)$ and $\tau^{\eta p}_{\xi k} = \tau^{\eta p}_{\xi k_F}$. We find $r = \sigma^{nd}_{xx}(\xi, \eta, p)/\sigma^d_{xx}(\xi, \eta, p) << 1$, mainly because $\sigma^{nd}_{xx}(\xi, \eta, p) \propto \Gamma$. The precise value of r depends on the scattering strength through Γ and τ appearing in $\sigma^d_{xx}(\xi, \eta, p)$. In what follows we neglect $\sigma^{nd}_{xx}(\xi, \eta, p)$.

After evaluating the integral over k, Eq. (25) becomes

$$\sigma^d_{xx}(\xi, \eta, p) = \frac{e^2\tau_F E_F}{\pi\hbar^2}\left[\left. Q^{\eta p}_{\xi}\frac{\theta(E_F - E^{\eta p}_{1g})}{1 - \bar{\lambda}^2/M}\right|_{\epsilon_{+F}}\right.$$
$$\left. + \left. Q^{\eta p}_{\xi}\frac{\theta(E_F - E^{\eta p}_{2g})}{1 + \bar{\lambda}^2/M}\right|_{\epsilon_{-F}}\right], \qquad (26)$$

where $Q^{\eta p}_{\xi} = (A^{\eta p}_{\xi} + B^{\eta p}_{\xi}C^{\eta p}_{\xi})^2(N^{\eta p}_{\xi})^4$ and $\tau_F \equiv \tau^{\eta p}_{\xi k_F}$ is the relaxation time evaluated at the Fermi level. As indicated, the 1st and 2nd line in the square brackets are to be evaluated at ϵ_{+F} and ϵ_{-F}, respectively, where $\epsilon_{\pm F}$ is obtained from Eq. (15) for $E = E_F$. To evaluate Eq. (25) numerically we used a Lorentzian broadening of $\delta(E^{\eta p}_{\xi} - E_F)$.

The valley P_v and spin P_s polarizations, corresponding to Eq. (25), are

$$P_v = \sum_{\xi p}\frac{\sigma^d_{xx}(l, s, +, p) - \sigma^d_{xx}(l, s, -, p)}{\sigma^d_{xx}(l, s, +, p) + \sigma^d_{xx}(l, s, -, p)}, \qquad (27)$$

and

$$P_s = \sum_{\eta pl}\frac{\sigma^d_{xx}(l, +, \eta, p) - \sigma^d_{xx}(l, -, \eta, p)}{\sigma^d_{xx}(l, +, \eta, p) + \sigma^d_{xx}(l, -, \eta, p)}. \qquad (28)$$

In Fig. 4 we plot the conductivity, given by Eq. (25), as a function of the Fermi energy E_F by evaluating the
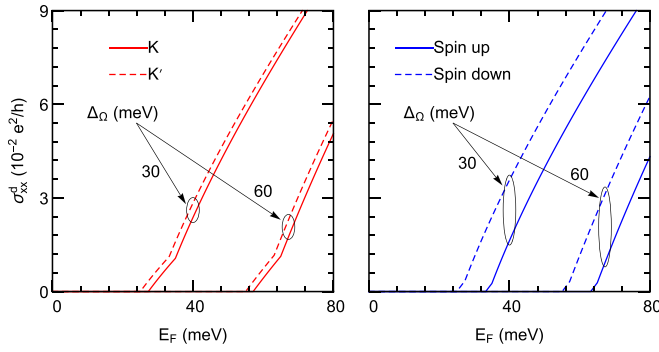
FIG. 4. Longitudinal conductivity vs Fermi energy E_F for $T = 0$ K, and $\tau_F = 1 \times 10^{-15}$ sec. The other parameters are the same as in Fig. 2.

integral over k numerically for two values of the parameter Δ_Ω and $p = +1$. Further, the left panel represents the valley-dependent contribution of Eq. (25), with both spins included, whereas the right one depicts its spin-dependent contribution with both valleys included. To display the result clearly, we set $\Delta = 1$ meV, $\lambda_R = 2$ meV, $\lambda_v = 4$ meV, and $\tau_F = 1 \times 10^{-15}$ sec. We find that $\sigma_{xx}^d(\xi, \eta, p)$ vanishes when E_F is in the gap while it increases linearly when E_F is outside the gap. The kink appears when E_F crosses the conduction band ($E_{++}^{\eta+}$). Moreover, we find $\sigma_{xx}^d(\xi, +, +) = \sigma_{xx}^d(\xi, -, +)$ in the inverted band regime ($\Delta_\Omega = 0$) while $\sigma_{xx}^d(\xi, +, +) \neq \sigma_{xx}^d(\xi, -, +)$ in the direct band regime ($\Delta_\Omega \neq 0$). We also verified that the analytical result [Eq. (26)] agrees well with the numerical one obtained from Eq. (25).

We plot the total longitudinal conductivity, with both valleys and spins included, in Fig. 5 for different values of Δ_Ω. As expected, σ_{xx}^d is an even function of Δ_Ω. In addition, the band gap increases with Δ_Ω.
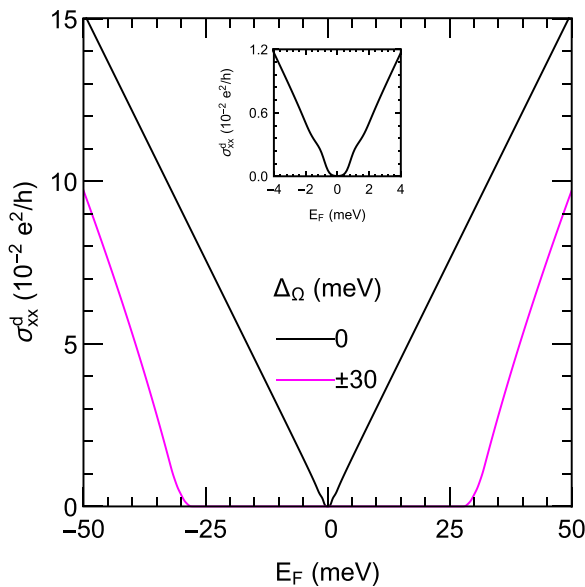

FIG. 5. Total longitudinal conductivity vs Fermi energy E_F. The parameters are $\Delta = 0.54$ meV, $\lambda_R = 0.56$ meV, and $\lambda_v = 1.22$ meV [57].
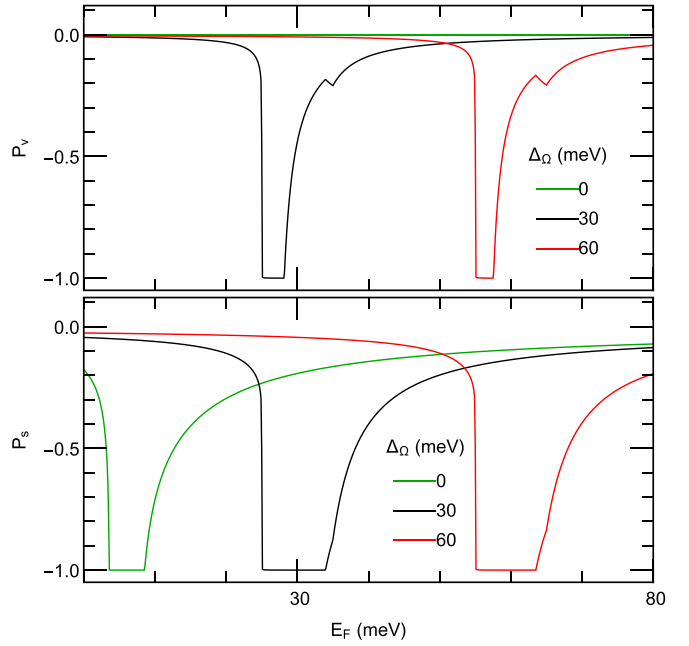

FIG. 6. Valley P_v and spin P_s polarization vs E_F for different values of Δ_Ω, as indicated, and $\lambda_R = 4$ meV. The other parameters are the same as in Fig. 4. Notice that $P_v = 0$ for $\Delta_\Omega = 0$ while $P_s \neq 0$.

The valley P_v and spin P_s polarizations versus E_F are shown in Fig. 6 for $\lambda_R = 4$ meV and three different values of Δ_Ω. It can be seen that $P_v = 0$ in the inverted band regime while $P_v \neq 0$ in the direct band one. In other words, the valley polarization can be switched on and off by controlling the parameter Δ_Ω. On the other hand, $P_s \neq 0$ in both band regimes. It is interesting to study P_v in the direct band regime ($\Delta_\Omega \neq 0$). The contribution of $\sigma_{xx}^d(\xi, +)$ to P_v is zero in the range $\lambda_v + \Delta - \Delta_\Omega \leqslant E_F < \lambda_v + \Delta + \Delta_\Omega$. Thus, $P_v = 1$, which is a pure K' valley polarization for $\Delta_\Omega \neq 0$. When we change the polarization of light to $p = -1$, a pure K valley polarization is obtained. That is, one can easily reverse the valley polarization by reversing that of the circularly polarized light. This result may be useful in valleytronics applications, such as making valley valves [71].

In Fig. 7 we show the numerically evaluated valley-Hall conductivity σ_{yx}^v, from Eq. (22), in the inverted ($\Delta_\Omega = 0$) and direct ($\Delta_\Omega \neq 0$) band regimes for $l = l'$ with $s \neq s'$, as well as for $l \neq l'$ with $s = s'$ and $s \neq s'$. We used a sufficiently low temperature ($T = 1$ K) to ensure that thermal vibrations of atoms have a negligible contribution to the electron transport. σ_{yx}^v is quantized and has the universal value $2e^2/h$ when the Fermi level is in the gap -1 meV $\leqslant E_F \leqslant 1$ meV (see green curve, compare with the DOS in Fig. 2). Its absolute value is reduced outside the gap as E_F increases. The two peaks, to the left and right of the gap, at $E_F \approx \pm 1.5$ meV, appear due to the inverted band structure or the Mexican hat-like dispersion as can be seen in the inset of Fig. 7. σ_{yx}^v vanishes when E_F is in the gap in the direct band regime $\Delta_\Omega \neq 0$ as the blue curve shows. The reason is that in this case electrons from both valleys flow in opposite directions and their contributions to the valley current exactly cancel each other.
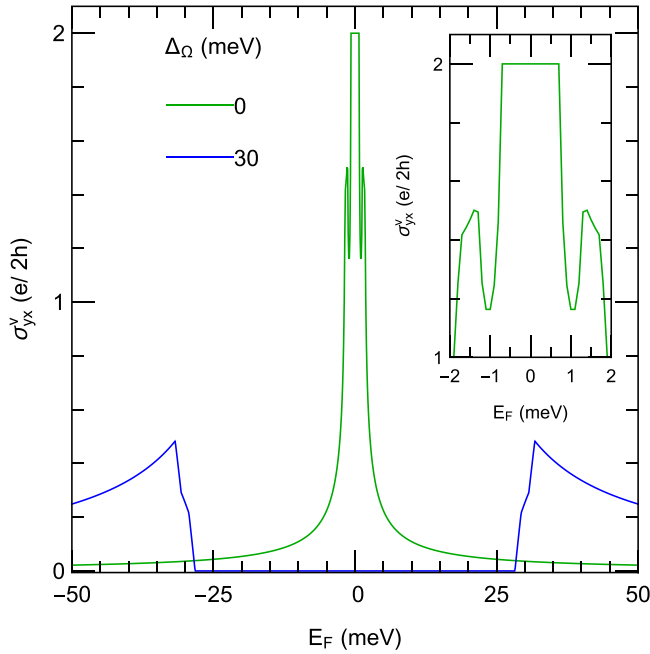
FIG. 7. Valley-Hall conductivity vs E_F for $T = 1$ K and $\Gamma = 0$. The other parameters are $\Delta = 0.54$ meV, $\lambda_R = 0.56$ meV, and $\lambda_v = 1.22$ meV [57]. The green curve is measured in units of e/h and the blue one in units of $e/10h$. The inset is a blowup of the region -2 meV $\leqslant E_F \leqslant 2$ meV.

FIG. 8. Charge Hall conductivity vs E_F for different values of Δ_Ω. The other parameters are the same as in Fig. 7. It vanishes for $\Delta_\Omega = 0$ and changes sign when Δ_Ω is changed to $-\Delta_\Omega$.

A non zero valley-Hall current is produced when E_F crosses the conduction and valence bands. When E_F grows further, the conductivity decreases. It is also worth noticing that the valley conductivity changes sign (not shown) if proximitized graphene is irradiated by a right circularly polarized light ($p = -1$).

For $\Delta_\Omega = 0$ a quantized valley-Hall conductivity of $2e^2/h$ is obtained in the band gap as can be seen from the green curve in the inset of Fig. 7. On the other hand, for $\Delta_\Omega \neq 0$ the valley-Hall conductivity is quenched to zero within the band gap (see the blue curve of Fig. 7), while a quantized charge Hall conductivity of $2e^2/h$ and $-2e^2/h$ is obtained for the left- and right-handed circularly polarized light, respectively, as shown in Fig. 8. The reason for the change $2e^2/h \rightarrow -2e^2/h$ is that this nondiagonal contribution to the conductivity is an odd function of Δ_Ω.

IV. SUMMARY AND CONCLUSIONS

We investigated the valley-dependent dc transport by employing the linear response formalism and Floquet theory in the high-frequency limit as well as the energy dispersion in the presence of proximity-induced gaps. We derived analytical expressions for the energy dispersion relation of Dirac fermions, the DOS, and the diagonal and nondiagonal parts of the conductivity. We found that a transition occurs from an inverted band regime to a direct one for $\Delta_\Omega > \Delta + \lambda_v$ (see Fig. 2). In addition, the energy dispersion shows a complete lifting of the *fourfold* spin and valley degeneracies in the direct band structure while it has a *twofold* valley degeneracy in the inverted band phase. We demonstrated that the DOS exhibits
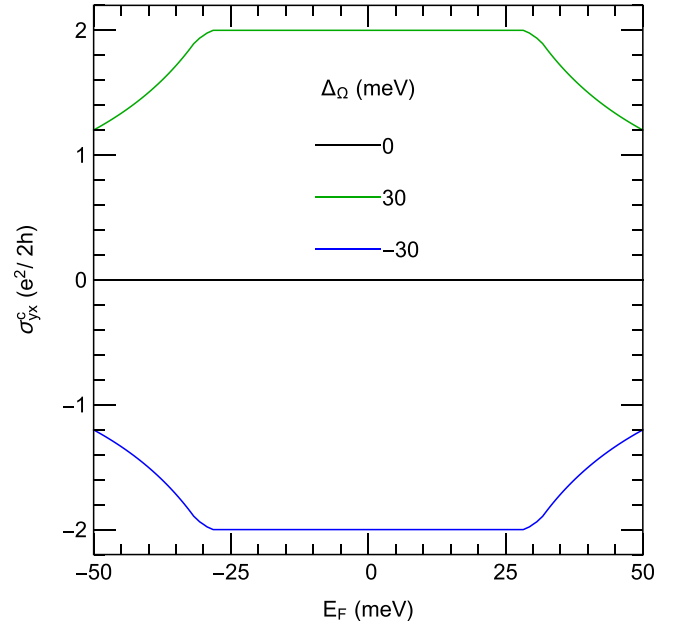
a van Hove singularity due to the inverted band structure, which remained unchanged as long as $\Delta_\Omega < \Delta + \lambda_v$. The four jumps in the DOS are due to the lifting of the *fourfold* spin and valley degeneracy in the direct band regime in contrast to pristine graphene, cf. Fig. 3.

We showed that the valley polarization P_v vanishes for $\Delta_\Omega < \Delta + \lambda_v$ while for $\Delta_\Omega > \Delta + \lambda_v$ it is finite, $P_v \neq 0$; this might be useful in the design of valleytronics devices such as optically controlled valley filters and valves based on proximitized graphene. On the other hand, $P_s \neq 0$ in both band regimes. Further, 100% K or K' valley polarization is achieved in the range $\lambda_v + \Delta - \Delta_\Omega \leqslant E_F < \lambda_v + \Delta + \Delta_\Omega$ when the handedness of the light polarization changes.

We found that, when E_F in the gap, $\sigma_{yx}^v = 2e^2/h$ in the invert band regime while $\sigma_{yx}^v = 0$ in the direct band regime. Peaks are found in the curve of σ_{yx}^v versus E_F when E_F crosses the inverted dispersion, see the green curve in Fig. 7. Moreover, for $\Delta_\Omega > \Delta + \lambda_v$, we have $\sigma_{yx}^v \neq 0$ when E_F crosses the conduction and valence bands. The valley-Hall conductivity tends to $\sigma_{yx}^v = 0$ for both invert and direct band regimes in the limit $E_F \rightarrow \pm\infty$. A last finding is that the charge Hall conductivity is finite for $\Delta_\Omega \neq 0$ and changes sign when the handedness of the light polarization changes.

Our results may be pertinent to developing future spintronics and valleytronics devices such as field-effect tunneling transistors, memory devices, phototransistors, etc.

[1] A. H. Castro Neto, F. Guinea, N. M. R. Peres, K. S. Novoselov, and A. K. Geim, Rev. Mod. Phys. **81**, 109 (2009).

[2] M. Gmitra, S. Konschuh, C. Ertler, C. Ambrosch-Draxl, and J. Fabian, Phys. Rev. B **80**, 235431 (2009).

[3] J. Sichau, M. Prada, T. Anlauf, T. J. Lyon, B. Bosnjak, L. Tiemann, and R. H. Blick, Phys. Rev. Lett. **122**, 046403 (2019).

[4] A. A. Kaverzin and B. J. van Wees, Phys. Rev. B **91**, 165412 (2015).

[5] J. Balakrishnan, G. K. W. Koon, M. Jaiswal, A. H. C. Neto, and B. C. Ozyilmaz, Nat. Phys. **9**, 284 (2013).

[6] X. Hong, S.-H. Cheng, C. Herding, and J. Zhu, Phys. Rev. B **83**, 085410 (2011).

[7] Z. Jia, B. Yan, J. Niu, Q. Han, R. Zhu, D. Yu, and X. Wu, Phys. Rev. B **91**, 085411 (2015).

[8] U. Chandni, E. A. Henriksen, and J. P. Eisenstein, Phys. Rev. B **91**, 245402 (2015).

[9] Y.-C. Lin, N. Lu, N. Perea-Lopez, J. Li, Z. Lin, X. Peng, C. H. Lee, C. Sun, L. Calderin, P. N. Browning *et al.*, ACS Nano **8**, 3715 (2014).

[10] M.-Y. Lin, C.-E. Chang, C.-H. Wang, C.-F. Su, C. Chen, S.-C. Lee, and S.-Y. Lin, Appl. Phys. Lett. **105**, 073501 (2014).

[11] A. Azizi, S. Eichfeld, G. Geschwind, K. Zhang, B. Jiang, D. Mukherjee, L. Hossain, A. F. Piasecki, B. Kabius, J. A. Robinson, and N. Alem, ACS Nano **9**, 4882 (2015).

[12] M. Gmitra and J. Fabian, Phys. Rev. B **92**, 155403 (2015).

[13] Z. Wang, D.-K. Ki, J. Y. Khoo, D. Mauro, H. Berger, L. S. Levitov, and A. F. Morpurgo, Phys. Rev. X **6**, 041020 (2016).

[14] T. Völkl, T. Rockinger, M. Drienovsky, K. Watanabe, T. Taniguchi, D. Weiss, and J. Eroms, Phys. Rev. B **96**, 125405 (2017).

[15] A. Avsar *et al.*, Nat. Commun. **5**, 4875 (2014).

[16] S. Omar and B. J. van Wees, Phys. Rev. B **95**, 081404(R) (2017).

[17] A. Dankert and S. P. Dash, Nat. Commun. **8**, 16093 (2017).

[18] M. Offidani, M. Milletarí, R. Raimondi, and A. Ferreira, Phys. Rev. Lett. **119**, 196801 (2017).

[19] S. Zihlmann, A. W. Cummings, J. H. Garcia, M. Kedves, K. Watanabe, T. Taniguchi, C. Schönenberger, and P. Makk, Phys. Rev. B **97**, 075434 (2018).

[20] J. H. Garcia, M. Vila, A. W. Cummings, and S. Roche, Chem. Soc. Rev. **47**, 3359 (2018).

[21] A. W. Cummings, J. H. Garcia, J. Fabian, and S. Roche, Phys. Rev. Lett. **119**, 206601 (2017).

[22] T. S. Ghiasi, J. Ingla-Aynés, A. A. Kaverzin, and B. J. van Wees, Nano Lett. **17**, 7528 (2017).

[23] L. A. Benítez, J. F. Sierra, W. Savero Torres, A. Arrighi, F. Bonell, M. V. Costache, and S. O. Valenzuela, Nat. Phys. **14**, 303 (2018).

[24] D. Kochan, S. Irmer, and J. Fabian, Phys. Rev. B **95**, 165415 (2017).

[25] D. N. Basov, R. D. Averitt, and D. Hsieh, Nat. Mater. **16**, 1077 (2017).

[26] F. Krausz and M. I. Stockman, Nat. Photon. **8**, 205 (2014).

[27] D. Fausti, R. I. Tobey, N. Dean, S. Kaiser, A. Dienst, M. C. Hoffmann, S. Pyon, T. Takayama, H. Takagi, and A. Cavalleri, Science **331**, 189 (2011).

[28] M. Mitrano, A. Cantaluppi, D. Nicoletti, S. Kaiser, A. Perucchi, S. Lupi, P. Di Pietro, D. Pontiroli, M. Riccó, S. R. Clark *et al.*, Nature (London) **530**, 461 (2016).

[29] M. Rini, A. Cavalleri, R. W. Schoenlein, R. López, L. C. Feldman, R. F. Haglund, L. A. Boatner, and T. E. Haynes, Opt. Lett. **30**, 558 (2005).

[30] M. Liu, H. Y. Hwang, H. Tao, A. C. Strikwerda, K. Fan, G. R. Keiser, A. J. Sternbach, K. G. West, S. Kittiwatanakul, J. Lu *et al.*, Nature (London) **487**, 345 (2012).

[31] E. Pomarico, M. Mitrano, H. Bromberger, M. A. Sentef, A. Al-Temimy, C. Coletti, A. Stöhr, S. Link, U. Starke, C. Cacho, R. Chapman, E. Springate, A. Cavalleri, and I. Gierz, Phys. Rev. B **95**, 024304 (2017).

[32] D. M. Kennes, E. Y. Wilner, D. R. Reichman, and A. J. Millis, Nat. Phys. **13**, 479 (2017).

[33] M. A. Sentef, Phys. Rev. B **95**, 205111 (2017).

[34] T. Oka and H. Aoki, Phys. Rev. B **79**, 081406(R) (2009).

[35] T. Kitagawa, T. Oka, A. Brataas, L. Fu, and E. Demler, Phys. Rev. B **84**, 235108 (2011).

[36] N. H. Lindner, G. Refael, and V. Galitski, Nat. Phys. **7**, 490 (2011).

[37] M. A. Sentef, M. Claassen, A. F. Kemper, B. Moritz, T. Oka, J. K. Freericks, and T. P. Devereaux, Nat. Commun. **6**, 7047 (2015).

[38] H. Hübener, M. A. Sentef, U. De Giovannini, A. F. Kemper, and A. Rubio, Nat. Commun. **8**, 13940 (2017).

[39] Y. H. Wang, H. Steinberg, P. Jarillo-Herrero, and N. Gedik, Science **342**, 453 (2013).

[40] F. Mahmood, C.-K. Chan, Z. Alpichshev, D. Gardner, Y. Lee, P. A. Lee, and N. Gedik, Nat. Phys. **12**, 306 (2016).

[41] H. Miyake, G. A. Siviloglou, C. J. Kennedy, W. C. Burton, and W. Ketterle, Phys. Rev. Lett. **111**, 185302 (2013).

[42] N. Fläschner, B. S. Rem, M. Tarnowski, D. Vogel, D.-S. Lühmann, K. Sengstock, and C. Weitenberg, Science **352**, 1091 (2016).

[43] M. C. Rechtsman, J. M. Zeuner, Y. Plotnik, Y. Lumer, D. Podolsky, F. Dreisow, S. Nolte, M. Segev, and A. Szameit, Nature (London) **496**, 196 (2013).

[44] M. Aidelsburger, S. Nascimbene, and N. Goldman, C. R. Phys. **19**, 394 (2018).

[45] T. Ozawa, H. M. Price, A. Amo, N. Goldman, M. Hafezi, L. Lu, M. Rechtsman, D. Schuster, J. Simon, O. Zilberberg, and I. Carusotto, Rev. Mod. Phys. **91**, 015006 (2019).

[46] L. Asteria, D. T. Tran, T. Ozawa, M. Tarnowski, B. S. Rem, N. Fläschner, K. Sengstock, N. Goldman, and C. Weitenberg, Nat. Phys. **15**, 449 (2019).

[47] J. W. McIver, B. Schulte, F.-U. Stein, T. Matsuyama, G. Jotzu, G. Meier, and A. Cavalleri, Nat. Phys. **16**, 38 (2020).

[48] S. A. Sato, J. W. McIver, M. Nuske, P. Tang, G. Jotzu, B. Schulte, H. Hübener, U. De Giovannini, L. Mathey, M. A. Sentef, A. Cavalleri, and A. Rubio, Phys. Rev. B **99**, 214302 (2019).

[49] M. Bukov, L. D'Alessio, and A. Polkovnikov, Adv. Phys. **64**, 139 (2015).

[50] L. E. F. Foa Torres, P. M. Perez-Piskunow, C. A. Balseiro, and G. Usaj, Phys. Rev. Lett. **113**, 266801 (2014).

[51] G. Usaj, P. M. Perez-Piskunow, L. E. F. Foa Torres, and C. A. Balseiro, Phys. Rev. B **90**, 115423 (2014).

[52] H. Dehghani, T. Oka, and A. Mitra, Phys. Rev. B **90**, 195429 (2014).

[53] A. Kundu, H. A. Fertig, and B. Seradjeh, Phys. Rev. Lett. **113**, 236803 (2014).

[54] M. Tahir, A. Manchon, and U. Schwingenschlögl, Phys. Rev. B **90**, 125438 (2014).

[55] T. Mikami, S. Kitamura, K. Yasuda, N. Tsuji, T. Oka, and H. Aoki, Phys. Rev. B **93**, 144307 (2016).

[56] M. Tahir and P. Vasilopoulos, Phys. Rev. B **91**, 115311 (2015).

[57] M. Gmitra, D. Kochan, P. Högl, and J. Fabian, Phys. Rev. B **93**, 155104 (2016).

[58] C. L. Kane and E. J. Mele, Phys. Rev. Lett. **95**, 226801 (2005); **95**, 146802 (2005).

[59] A. M. Alsharari, M. M. Asmar, and S. E. Ulloa, Phys. Rev. B **98**, 195129 (2018).

[60] Z. Wang, D. K. Ki, H. Chen, H. Berger, A. H. MacDonald, and A. F. Morpurgo, Nat. Commun. **6**, 8339 (2015).

[61] B. Yang, M.-F. Tu, J. Kim, Y. Wu, H. Wang, J. Alicea, R. Wu, M. Bockrath, and J. Shi, 2D Mater. **3**, 031012 (2016).

[62] C. J. Tabert and E. J. Nicol, Phys. Rev. B **87**, 235426 (2013).

[63] E. J. Nicol and J. P. Carbotte, Phys. Rev. B **77**, 155409 (2008).

[64] M. Charbonneau, K. M. Van Vliet, and P. Vasilopoulos, J. Math. Phys. **23**, 318 (1982).

[65] T. Iadecola, T. Neupert, and C. Chamon, Phys. Rev. B **91**, 235133 (2015).

[66] C. J. Tabert and E. J. Nicol, Phys. Rev. Lett. **110**, 197402 (2013); Phys. Rev. B **88**, 085434 (2013).

[67] K. Shakouri, P. Vasilopoulos, V. Vargiamidis, and F. M. Peeters, Phys. Rev. B **90**, 235423 (2014).

[68] M. Tahir, P. M. Krstajić, and P. Vasilopoulos, Phys. Rev. B **98**, 075429 (2018); Phys. Rev B **95**, 235402 (2017).

[69] C. K. Safeer, J. Ingla-Aynés, F. Herling, J. H. Garcia, M. Vila, N. Ontoso, M. Reyes Calvo, S. Roche, L. E. Hueso, and F. Casanova, Nano Lett. **19**, 1074 (2019).

[70] D. Xiao, W. Yao, and Q. Niu, Phys. Rev. Lett. **99**, 236809 (2007).

[71] A. Rycerz, J. Tworzydlo, and C. Beenakker, Nat. Phys. **3**, 172 (2007).